μSR and magnetometry study of the type-I superconductor BeAu

J. Beare,[1] M. Nugent,[1] M. N. Wilson,[1] Y. Cai,[1] T. J. S. Munsie,[1] A. Amon,[2] A. Leithe-Jasper,[2] Z. Gong,[3] S. L. Guo,[4] Z. Guguchia,[3] Y. Grin,[2] Y. J. Uemura,[3] E. Svanidze,[2] and G. M. Luke[1,5,6]

[1]*Department of Physics and Astronomy, McMaster University, Hamilton, Ontario, Canada L8S 4M1*
[2]*Max-Planck-Institut für Chemische Physik fester Stoffe, Nöthnitzer Straße 40, 01187 Dresden, Germany*
[3]*Department of Physics, Columbia University, New York, New York 10027, USA*
[4]*Department of Physics, Zhejiang University, Hangzhou 310027, China*
[5]*Canadian Institute for Advanced Research, Toronto, Ontario, Canada M5G 1Z7*
[6]*TRIUMF, Vancouver, British Columbia, Canada V6T 2A3*

We present muon spin rotation and relaxation (μSR) measurements as well as demagnetizing-field-corrected magnetization measurements on polycrystalline samples of the noncentrosymmetric superconductor BeAu. From μSR measurements in a transverse field, we determine that BeAu is a type-I superconductor with $H_c = 258$ Oe, amending the previous understanding of the compound as a type-II superconductor. To account for demagnetizing effects in magnetization measurements, we produce an ellipsoidal sample, for which a demagnetization factor can be calculated. After correcting for demagnetizing effects, our magnetization results are in agreement with our μSR measurements. Using both types of measurements, we construct a phase diagram from $T = 30$ mK to $T_c \approx 3.25$ K. We then study the effect of hydrostatic pressure and find that 450 MPa decreases T_c by 35 mK, comparable to the change seen in the type-I elemental superconductors Sn, In, and Ta. This suggests BeAu is far from a quantum critical point accessible by the application of pressure.

I. INTRODUCTION

The absence of inversion symmetry in noncentrosymmetric superconductors results in an antisymmetric spin-orbit coupling, which splits otherwise degenerate electronic bands [1]. Parity of the superconducting parameter is no longer conserved, allowing spin-singlet and spin-triplet states to mix. These mixed-parity states are generally expected to give rise to point or line nodes in the superconducting gap [2–4].

Evidence for line nodes has been found in CePt$_3$Si [5], CeIrSi$_3$ [6], Mg$_{10}$Ir$_{19}$B$_{16}$ [7], Mo$_3$Al$_2$C [8], and Li$_2$Pt$_3$B [9], while many other noncentrosymmetric superconductors possess fully gapped states [10–15]. Other noncentrosymmetric superconductors such as La$_2$C$_3$ [16] and TaRh$_2$B$_2$ exhibit multigap behavior. A detailed analysis of the possible pairing mechanisms [17] shows that either isotropic or nodal gaps are possible, depending on the anisotropy of the pairing mechanism. The anisotropy may depend upon the strength of spin-orbit coupling in the material [10].

In addition to breaking parity symmetry, noncentrosymmetric superconductors can also exhibit time-reversal symmetry breaking. Muon spin rotation and relaxation (μSR) has been used to detect time-reversal symmetry breaking in the noncentrosymmetric superconductors Re$_6$D (D = Zr, Hf, Ti) [18–20], La$_7$Ir$_3$ [13], LaNiC$_2$ [14], and SrPtAs [21] as well as several centrosymmetric superconductors [22–29]. Further study of noncentrosymmetric superconductors, such as BeAu, is required to probe the unconventional pairing mechanisms and explore the diverse gap properties that have been exhibited.

BeAu exhibits cubic space-group symmetry of $P2_13$ (FeSi) with lattice parameter $a = 4.6699(4)$ Å. From previous work

[30], BeAu exhibits conventional Bardeen-Cooper-Schrieffer-type superconductivity below $T_c \approx 3.3$ K with a full Meissner flux expulsion. The specific heat jump at the superconducting transition is equal to the normal state-specific heat, indicating bulk superconductivity. BeAu can be classified as a weakly coupled superconductor with $\Delta C/\gamma_n T_c \approx 1.26$, $\lambda_{e-p} = 0.5$, and $2\Delta(0)/k_B T_c = 3.72$. Previously [30], BeAu was thought to be a type-II superconductor with lower critical field $H_{c1} = 32$ Oe and upper-critical field $H_{c2} = 335$ Oe based upon magnetization measurements which used a spherical demagnetization factor $N = \frac{1}{3}$ when measuring an irregularly shaped sample. This is a common first assumption when correcting for demagnetizing effects that we would like to improve upon in this paper. Zero-field μSR measurements presented in Ref. [30] show no time-reversal symmetry breaking.

μSR is a powerful technique which can be used to measure internal fields due to time-reversal symmetry breaking as well as give an accurate measurement of the penetration depth and coherence length of type-II superconductors. As muons are a local probe of magnetism, μSR is insensitive to the large demagnetizing fields produced outside of superconductors. In this paper, transverse field (TF) μSR measurements are used to demonstrate that BeAu is a type-I superconductor with $H_c = 258$ Oe. Demagnetizing effects in superconductors can cause parts of a sample to experience a magnetic field that is larger than the applied field. If the local field due to demagnetizing effects at the surface of a type-I superconductor is above H_c, then at least part of the sample will enter the normal state. In this situation, the free energy is minimized by a complicated structure of alternating normal and superconducting regions which depends upon the geometry

of the sample, as well as the coherence length and penetration depth [31–33]. This is known as the intermediate state of a type-I superconductor and occurs for applied fields, H_a, between $(1 - N) H_c$ and H_c, where N is the demagnetization factor of the sample. At low applied fields, close to $(1 - N)$ H_c, the free energy of the intermediate state is minimized when the normal regions of the sample have an internal field of H_c. At high magnetic fields, close to H_c, interface effects between normal and superconducting regions, as well as surface effects, modify the thermodynamic critical field to a slightly reduced value H_{cI} [31–33]. The magnetic moment of a muon landing within a type-I superconductor will therefore either be stationary in the superconducting regions (where the field is zero) or will precess in a field very close to H_c in the normal regions. The probability that a muon experiences either field is equal to the volume fraction of the sample in the respective states and, therefore, a μSR measurement directly measures the superconducting volume fraction of the sample.

μSR has been used to study elemental type-I superconductors such as Sn (IV) [34] and we find qualitatively similar results in BeAu. The most striking indication of type-I behavior in BeAu is that, below T_c, the normal regions of the sample have a relatively constant value of the internal field of $H_c = 258$ Oe, for all applied fields between 50 Oe and 250 Oe. This can be contrasted with the expected internal field behavior of the vortex state of a type-II superconductor, where the internal field distribution in the normal cores falls mostly below the applied field and, in general, changes as a function of the applied field. BeAu joins a relatively small list of nonelemental compounds which show type-I behavior [12,35–42].

Our μSR results call for a more accurate accounting of demagnetizing effects in magnetization measurements to reconcile previous magnetization measurements [30] with the identification of BeAu as a type-I superconductor. To this end, a sample of BeAu is shaped into an ellipsoid so demagnetizing effects can be accounted for more accurately than is typically done in magnetization studies of superconductors. Using this geometry, a demagnetizing factor for the sample can be calculated which allows us to determine the internal field of the normal regions and demonstrate the type-I nature of this compound with magnetization measurements.

Pressure can often have a dramatic effect on superconductivity, especially when the system is near a quantum critical point. Cerium-based noncentrosymmetric superconductors have shown unusual behavior under the application of pressure with a pressure-induced superconducting transition discovered in CeIrGe$_3$, CeCoGe$_3$, and CeRhSi$_3$ [43–45], while CePt$_3$Si shows a strongly decreasing critical temperature as a function of applied pressure with a complete loss of superconductivity at 1.5 GPa [46]. Iron pnictide superconductors have also shown exotic behavior under the application of pressure [47]. This can be compared to elemental type-I superconductors which typically have a small decrease in T_c with the application of pressure but no exotic behavior is observed [48]. To compare BeAu to these cases, we study the effect of hydrostatic pressure and find that at 450 MPa BeAu still exhibits type-I behavior with a decrease in T_c of

35 mK. This decrease in T_c is similar to the change seen in type-I elemental superconductors such as Sn, In, and Ta under the same conditions [48] and suggests that BeAu is far from a quantum critical point that can be accessed by applying pressure.

II. EXPERIMENTAL METHODS

Polycrystalline samples were synthesized by arc melting from elemental Be (Heraeus, $\geqslant$99.9 wt.%) and Au (Alfa Aesar, $\geqslant$99.95 wt.%) in a 51:49 ratio, with mass loss of less than 0.3%. A small excess of beryllium was added to compensate for the Be loss due to evaporation. After melting, the boule was annealed in an argon atmosphere for 48 hours at 400 °C. A representative sample was measured to have a residual resistivity ratio of 38, which demonstrates the high purity of our samples. Further details can be found in Ref. [30].

Transverse field (TF) muon spin rotation and relaxation (μSR) measurements were performed on the M15 and M20 beamlines at the TRIUMF Laboratory in Vancouver, Canada. A spectrometer incorporating a dilution refrigerator was used on the M15 beamline, which allows for measurements in the temperature range of 0.025–10 K. The experimental setup makes use of a superconducting magnet to allow for fields up to 5 T. Samples were mounted on a silver cold finger to ensure good thermal conductivity and to give a well-defined μSR background signal with minimal relaxation. The instrument has a time resolution of 0.4 ns. The field was applied parallel to the direction of the muon beam and measurements were taken with the initial muon spin direction perpendicular to the field (TF). Several approximately elliptical discs of BeAu, each 0.5 mm thick and roughly 2.75 mm x 3.75 mm, were mounted on the cold finger such that a large fraction of the muon beam spot was covered. The direction of the applied field was perpendicular to the flat faces of the samples. Copper coil electromagnets were used to compensate for any stray fields. The LAMPF spectrometer was used on the M20 beamline, which allows measurements in the temperature range from 2–300 K in an applied field up to 0.4 T. A silver cold finger is not required on LAMPF and the background signal is greatly reduced. Thin, aluminum-backed mylar was used to mount a mosaic of BeAu discs to a copper square cutout. The experiment on M20 was performed using a similar TF setup as on M15. The μSRfit software package was used to analyze the μSR data [49].

Magnetometry measurements were taken at McMaster University using a Quantum Design XL-5 MPMS, which allows for measurements from 1.8 K to 300 K. We used a GC10/3 helium gas pressure cell from the Institute of High Pressure Physics, Polish Academy of Sciences, inserted into the MPMS to allow for magnetometry measurements under pressure up to 700 MPa, above 2 K. A 102.5 mg, nearly ellipsoidal sample with $a = b = 2.75$ mm and $c = 1.90$ mm was produced through grinding with a spherically concave, diamond Dremel head in a fume hood while submerged in mineral oil. A small section on either side of the c axis is flat due to the constraint of grinding while submerged in mineral oil to avoid the dispersal of toxic Be/BeO dust. The sample was measured in the MPMS at ambient pressure after which it needed to be ground down (under the same conditions) to
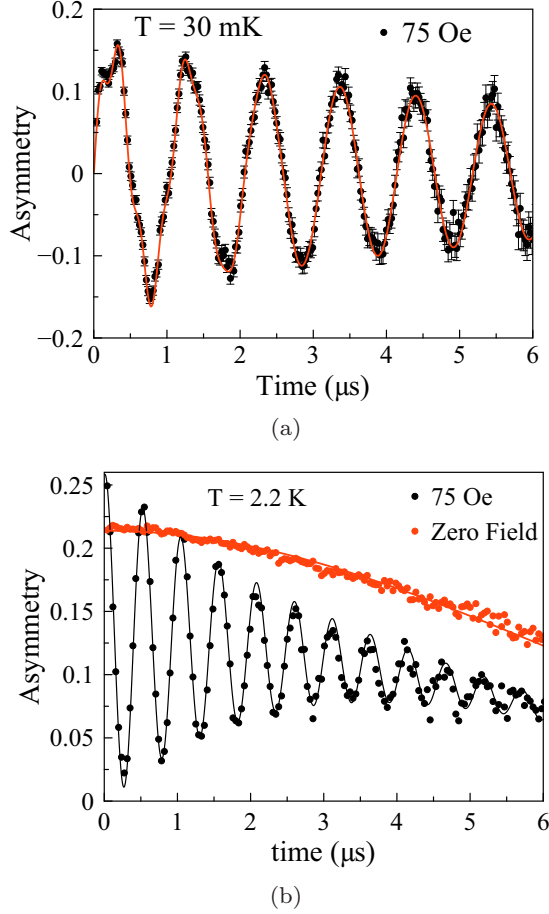
FIG. 1. (a) BeAu μ SR Asymmetry at 30 mK on the M15 beamline in an applied transverse field of 75 G showing two oscillating components, one from the sample and one from the sample holder. (b) μSR Asymmetry at 2.2 K on the M20 beamline in an applied transverse field of 75 G (black) and zero field (red). The nonoscillating component of the 75 G data relaxes with the same rate as the zero field data, showing that there are regions in the sample which are superconducting.

$a = b = 2.69$ mm and $c = 1.86$ mm to fit inside the 3-mm-diameter pressure cell.

III. RESULTS AND DISCUSSION

Figure 1(a) shows the TF μSR asymmetry spectrum at 30 mK on the M15 beamline while Fig. 1(b) shows the asymmetry spectrum on M20 at 2.2 K (black circles), both after field cooling in an applied field of 75 G. All μSR data presented is field cooled (FC). The M15 data show large oscillations as expected for muons precessing in the applied TF with additional contributions coming from a fraction of muons precessing in a different field. This is due to a significant fraction of muons stopping in the silver cold finger and precessing in the applied magnetic field while another fraction of muons stop in the sample and precess in the local field of the sample. The M15 data show a reduced initial asymmetry, A_0, while in a superconducting state due to there being no detectors in the direction of the initial muon polarization when using the TF geometry on M15. Muons landing in the

superconducting regions of the sample will not precess and their decay products, which tend to travel in the direction of the muon spin polarization, will be less likely to be detected. This reduces A_0 in the intermediate state of a type-I superconductor compared to the normal state. By comparing the initial asymmetry in the intermediate state and in the normal state, the superconducting volume fraction can be determined. In the intermediate state of a type-I superconductor, the μSR asymmetry measures the total fraction of the signal coming from the sample, F, as well as from superconducting regions in the sample, F_S, and the asymmetry spectrum on the M15 beamline may be fit to

$$A(t) = A_0 \{ F(1 - F_S) \cos(\gamma_\mu H_N + \phi) \exp\left(-\tfrac{1}{2}(\sigma_N t)^2\right)$$
$$+ (1 - F) \cos(\gamma_\mu H_{bkg} + \phi) \exp(-\lambda_{bkg} t) \}, \quad (1)$$

where A_0 is the initial asymmetry, H_N the internal field in the normal regions of the sample, H_{bkg} the background field seen by muons stopping outside of the sample, ϕ the phase shift in the μSR asymmetry, σ_N the relaxation rate of the normal regions of the sample, and σ_{bkg} the relaxation rate of muons stopping outside of the sample. As μSR samples the entire volume of the material, the fraction of the signal coming from normal/superconducting regions is equivalent to the volume fraction of the sample in the normal/superconducting state. To determine A_0 and to account for extrinsic effects, high temperature (above T_c) data was taken for each applied field and fits to Eq. (1) were performed after fixing $F_S = 0$. The missing asymmetry when comparing low temperature and high temperature measurements allows F_S to be determined on the M15 beamline. A fit to Eq. (1) at 30 mK and 75 G is given by the solid line in Fig. 1(a).

LAMPF on M20 has detectors in the direction of the initial muon polarization and the 75 Oe data [Fig. 1(b)] shows a large fraction of the signal is very slowly relaxing, which is expected if a large fraction of the signal is coming from superconducting regions with zero field. The relaxation rate of this nonoscillating component is equal to the relaxation rate of measurements performed in zero applied field and so this component may be identified with regions of the sample that are superconducting. The visual difference in relaxation rate between the 75 G and zero field measurements in Fig. 1(b) is due to the different initial asymmetries of the two types of measurements. The oscillating component of the signal comes from normal regions of the superconductor that are experiencing a nonzero field. There is very little background signal on M20 and the M20 asymmetry may be fit to

$$A(t) = A_0 \{ (1 - F_S) \cos(\gamma_\mu H_N + \phi) \exp(-\lambda_N t)$$
$$+ F_S \left(\tfrac{1}{3} + \tfrac{2}{3}(1 - (\sigma_S t)^2) \exp\left(-\tfrac{1}{2}(\sigma_S t)^2\right)\right) \}, \quad (2)$$

where A_0 is the initial asymmetry, F_S is the superconducting volume fraction, H_N and λ_N are the internal field and relaxation in the normal regions of the sample, ϕ the phase shift of the normal regions, and σ_S the relaxation rate of the superconducting regions of the sample. A fit to Eq. (2) at 2.2 K and 75 G is given by the solid line in Fig. 1. The relaxation rate, σ_S, is consistent with the zero applied field relaxation rate of 0.115 ± 0.002 μs^{-1} for all applied fields, demonstrating that these regions have zero internal field and

are truly superconducting. To determine the expected behavior of the internal field and superconducting volume fraction, a discussion of type-I superconductors is required.

For applied fields, H_a above $(1 - N)H_c$, where N is the demagnetization factor of the sample, demagnetizing fields cause regions of the surface of a type-I superconductor to experience a field that is larger than the critical field H_c, inevitably causing parts of the sample to enter the normal state. For applied fields $H_c(1 - N) \leqslant H_a \leqslant H_c$ a type-I superconductor will have a complicated structure of coexisting superconducting and normal regions known as the intermediate state. Just above approximately $(1 - N)H_c$, it can be shown that equilibrium between the superconducting and normal phases can only be achieved if the normal regions have an internal magnetic field of H_c [31,32,50,51]. The field changes from 0 in the superconducting state to H_c over a distance $\delta \approx \xi - \lambda_L$, where ξ is the coherence length and λ_L the London penetration depth, which requires energy. There is also a surface energy associated with maintaining the normal regions at H_c in an applied field of H_a. As the applied field increases, more normal regions are generated, increasing the energy requirements of both affects that slightly reduces the thermodynamic critical field from H_c to the intermediate critical field H_{cI}. In the case of a thin plate oriented perpendicular to H_a, under the assumption of a laminar domain structure of normal and superconducting regions, H_{cI} is approximated by

$$H_{cI} \approx H_c \left[1 - 2\theta \left(\frac{\delta}{d} \right)^{1/2} \right], \quad \theta = \sqrt{\frac{\ln 2}{\pi}}, \qquad (3)$$

where d is the plate thickness, δ the thickness of the interface between superconducting and normal regions, and θ is a numerical constant which depends on the assumed domain structure of the superconducting-normal regions as well as the geometry of the sample [31–33]. Similar effects will also slightly raise the Meissner to intermediate state transition field from $(1 - N)H_c$ [33].

To complicate matters more, the structure of superconducting-normal domains which minimizes the free energy changes as a function of H_a. At applied fields just above $\approx H_{cI}(1 - N)$ the free energy is minimized by having tubular-threadlike normal regions pierce the superconductor, while at intermediate fields the free energy is minimized by having corrugated laminae of superconducting and normal layers. Finally, at fields close to H_{cI}, tubular-threadlike superconducting regions pierce normal metal [31–33,50,52]. This behavior has been observed before [53–55], but the exact behavior of a material in the intermediate state is hard to predict *a priori* as it has been shown that the free-energy differences of various spatial configurations of the intermediate state are quite small. Observationally, the spatial configuration selection depends upon the exact experimental conditions, as well as sample quality [32,50,55].

The internal field in the normal regions of a type-I superconductor remain relatively constant at H_c until an applied field comparable with H_c is reached. A TF μSR experiment on a type-I superconductor, in an applied field above $H_c(1 - N)$ and sufficiently far below H_c, will therefore show muons in the normal regions of the sample precessing with a frequency distribution centered around $\omega = \gamma_\mu H_c$ where $\frac{\gamma_\mu}{2\pi} =$
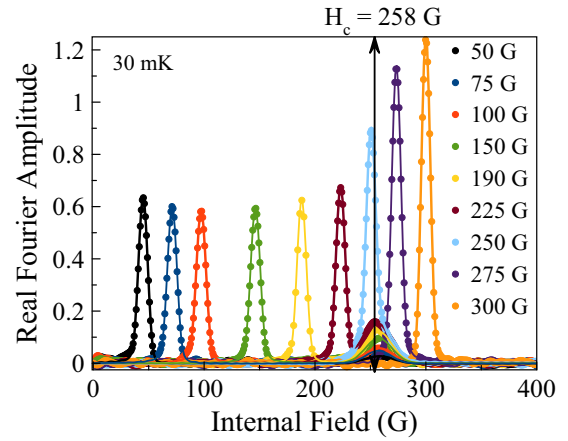
FIG. 2. The Fourier transform of the M15 μSR Asymmetry for a variety of fields at 30 mK. The sharp peaks in the data as well as color indicate the applied field experienced by muons stopping in the silver cold finger. The broad peak centered around 258 Oe for all applied fields below $H_a = 260$ Oe unambiguously shows BeAu to be a type-I superconductor.

135 MHz/T is the gyromagnetic ratio of the muon [56]. This can be contrasted with the expected results of a TF μSR experiment on a type-II superconductor in the vortex state where muons will precess at a frequency $\omega = \gamma_\mu H_{int}$ where H_{int} is an asymmetric distribution, the peak of which falls below H_a [56]. It should also be noted that while a type-I superconductor in the intermediate state will have an approximately constant internal field with $H_{int} \approx H_c$ or $H_{int} = 0$ (normal versus superconducting regions) for all applied fields in the range $H_c(1 - N) \leqslant H_a \leqslant H_c$, the peak position and shape of the H_{int} distribution for a type-II superconductor in the vortex state will generally depend upon H_a.

The Fourier transform of the μSR spectra gives the probability distribution of H_{int} in both the intermediate state of a type-I superconductor and the vortex state of a type-II superconductor. The probability distribution for both types of superconductors will show a sharp background peak at H_a on the M15 beamline from muons stopping in the silver cold finger but the internal field in a type-I superconductor will not change as a function of applied field. A type-II superconductor, however, will have a varying internal field. The short, broad peak centered at 258 Oe for all applied fields $H_a \leqslant 260$ G in Fig. 2 unambiguously demonstrates that BeAu is a type-I superconductor with $H_c \approx 258$ Oe.

The results from fitting the 30 mK data at various applied magnetic fields in the time domain are shown in Fig. 3. The superconducting volume fraction of the sample in the intermediate state of a type-I superconductor should decrease from 100% near $(1 - N)H_c$ approximately linearly, for low applied fields [32]. As the applied field increases and approaches H_{cI}, the superconducting volume fraction picks up a small correction given by Eq. (2.28) of Ref. [32]. The superconducting volume fraction for BeAu given in Fig. 3(a) shows qualitatively similar behavior to Ref. [34] and follows the expected linear behavior for fields not too close to H_c [31,32]. Figure 3(b) shows that the internal field in the normal regions of the sample is nearly constant as a function of

(a)

(b)
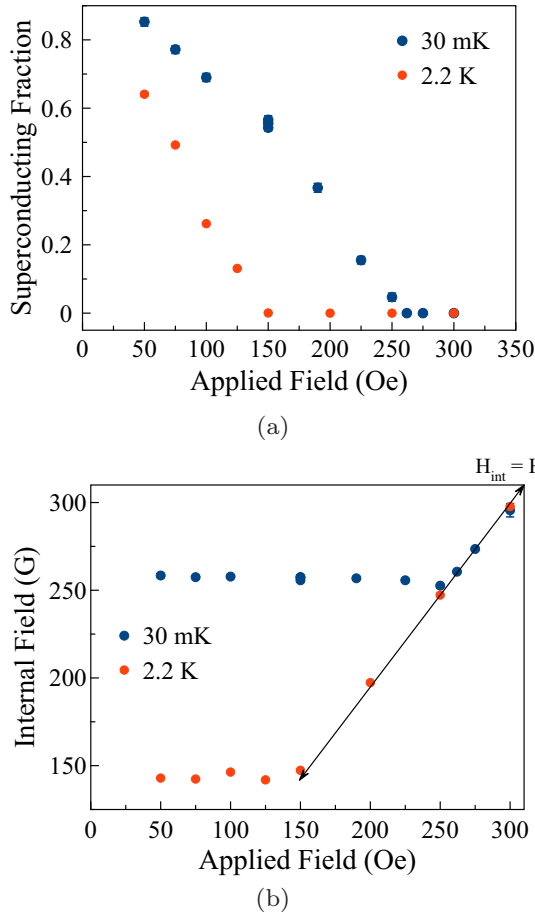
FIG. 3. (a) The superconducting volume fraction of the sample as a function of applied field at 30 mK after field cooling on M15 (blue) and 2.2 K on M20 (red). The superconducting volume fraction increases as the field decreases, as is expected for a type-I superconductor in the intermediate state. Where not shown, uncertainties are smaller than marker size. (b) The internal field in the normal regions of the sample as a function of applied field at 30 mK after field cooling on M15 (blue) and 2.2 K on M20 (red). The data shows the normal regions have an approximately constant internal field while in the intermediate state. For applied fields above H_{cI}, $H_{int} = H_a$, indicating the sample is in the normal state.

H_a until $H_a \approx H_{cI}$ is reached. Figure 3(b) also demonstrates that the thermodynamic critical field at 30 mK is slightly decreased from $H_c \approx 258 \pm 1$ Oe in an applied field of 50 Oe to $H_{cI} \approx 252.6 \pm 0.4$ Oe in an applied field of 250 Oe, in qualitative agreement with Eq. (3) and the expected behavior from Ref. [32]. The variation in internal field is due to the contribution of the interface energy between normal and superconducting regions as well as the interface energy between normal regions and regions outside the sample as a significant fraction of the sample enters the normal state [31–33,50,52].

Our 30 mK data show that BeAu is in the intermediate state from 50–250 Oe with some variability in internal field due to interface energy between normal and superconducting regions. The transition to the normal state above $\approx$250 Oe is indicated in Fig. 3(a) and indirectly shown in Fig. 3(b) where $H_{int} = H_a$ above 250 Oe. An approximate demagnetization factor of the measured discs is taken from a table [57] and

(a)

(b)
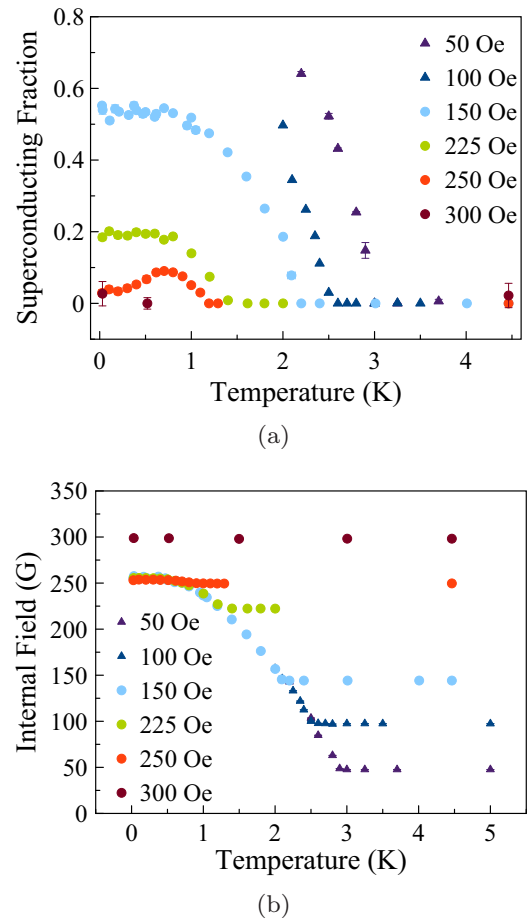
FIG. 4. (a) Superconducting volume fraction as a function of temperature. Data was taken after field cooling to base and measured upon heating to the specified temperature. Triangles indicate data was taken on M20 while circles indicate data was taken on M15. The superconducting volume fraction increases as the temperature decreases for fields below H_{cI}, as is expected for a type-I superconductor in the intermediate state. Uncertainties are smaller than marker size where not shown. (b) The internal field in the normal regions of the sample as a function of temperature. For an applied field below $H_{cI}(T)$, the internal field is equal to approximately $H_c(T)$ and μSR is able to measure $H_c(T)$ while in the intermediate state. For applied fields above $H_c(T)$, the sample is in the normal state and the internal field is equal to the applied field.

gives $N = 0.82$. Using $H_{M-I} \approx H_{cI}(1 - N)$ shows the Meissner state is expected for H_a less than $\approx$46 Oe. As we did not measure below 50 Oe, a pure Meissner state is not seen in our M15 data.

The μSR asymmetry of BeAu was also studied as a function of temperature for the applied fields 50 G, 100 G, 150 G, 225 G, 250 G, 300 G, and results are shown in Fig. 4. The fraction of the sample in the Meissner state generally increases as temperature decreases [Fig. 4(a)], as is expected in a type-I superconductor. The exception to this is the 250 G data set which peaks near 0.7 K, however, the applied field is close enough to $H_c(T = 0)$ that the superconducting-normal domain structure may change as a function of temperature, altering the relative size of the normal and superconducting volumes. The internal field in the normal regions as a function

of temperature is shown in Fig. 4(b) and demonstrates that the μSR technique can be used to trace out a partial H versus T phase diagram for type-I superconductors while in the intermediate state, i.e., when $H_{cI}(1 - N) \lesssim H_a \lesssim H_{cI}$.

Our μSR results unambiguously show that BeAu is a type-I superconductor, motivating a new careful study of the magnetization properties of BeAu using a well-defined sample geometry so that demagnetizing effects can be accounted for more accurately than is typically done in studies of superconductors. For a type-I superconductor of an ellipsoidal shape, the field at the surface of the equator of the sample, H_{eq}, when measuring in an applied field perpendicular to this equator, is given by

$$H_{eq} = H_a - 4\pi NM, \tag{4}$$

where N is the demagnetizing factor and M the magnetization of the sample [31,32,50]. An ellipsoid of revolution is one of the few shapes for which the demagnetization factor can be calculated analytically, which is why we produced a sample with this geometry [57,58]. The surface field at the equator of a superconducting ellipsoid is the maximum field that the sample experiences and is given by

$$H_{eq} = \frac{H_a}{1 - N}[31, 32]. \tag{5}$$

H_{eq} is an important quantity because, while in the intermediate state, the internal field is equal to the surface field on the equator of the superconductor. As this is the region with the highest local field, when the sample enters the normal state the equator should be the first region to do so. By using the fact that $H_{eq} = H_c$ while in the intermediate state, we should be able to reconstruct the discontinuous magnetization behavior expected at H_c for a type-I superconductor. An ellipsoidal type-I superconductor will be in the Meissner state below $H_a \approx (1 - N)H_{cI}$, above which it will enter the intermediate state [31,32]. Figure 5(a) shows the magnetization as a function of applied field for temperatures from 0.5 K to 3.2 K. Measurements were taken from 0 G to a maximum field, followed by measurements from the maximum field to 0 G. Fields are accurate to 0.1 G. Figure 5(a) shows linear behavior at low fields while in the Meissner state, with a departure from linearity as the minima is approached. The behavior is well described by a type-I superconductor entering the intermediate state near the magnetization minima followed by a transition to the normal state at high fields. The departure from linearity as the minima is approached is due to the generation of normal regions and the restructuring of normal-superconducting domains as the sample enters the intermediate state [33,52].

H_{eq} has very different behaviors for type-I superconductors in the intermediate state and type-II superconductors in the vortex state. In the intermediate state, the superconducting volume fraction of the sample decreases approximately linearly for a wide range of applied fields while the microscopic magnetization does not change. The linear decrease in the superconducting volume makes the overall magnitude of the magnetization of the entire sample decrease linearly. H_{eq} therefore remains constant, equal to internal field while in the intermediate state of a type-I superconductor.

(a)

(b)
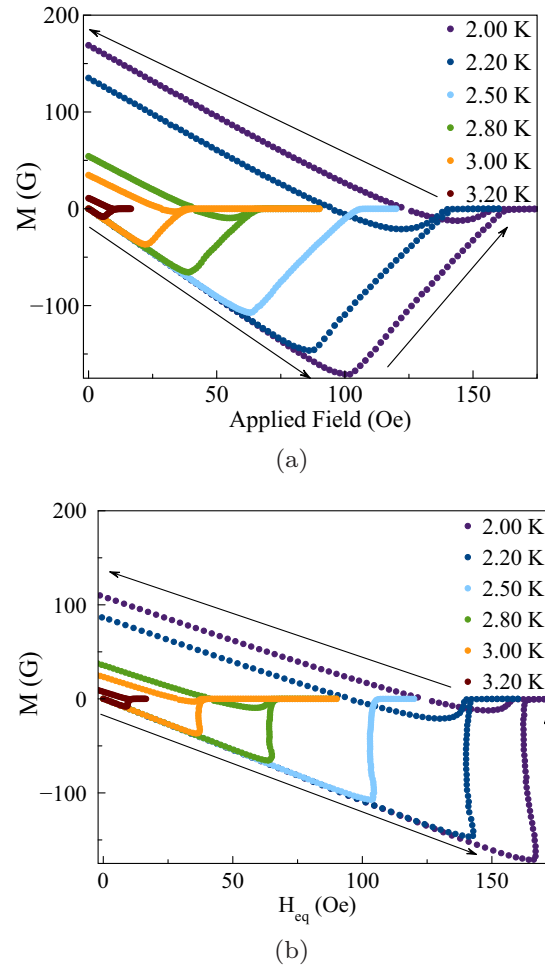
FIG. 5. (a) Magnetization as a function of applied field from 2.0 K to 3.2 K. Measurements were taken in increasing field followed by measurements in decreasing field once $H_{eq} > H_{cI}$ was reached. (b) Magnetisation as a function of the field at the equator $H_{eq} = H_a - 4\pi NM$. This plot shows the expected discontinuous transition in magnetization for a type-I superconductor.

A demagnetizing factor of $N_{ellipsoid} = 0.4355$ was calculated using Eq. (34) of Ref. [58], assuming the sample was a perfect ellipsoid with major-axis $a = b = 2.75$ mm and minor-axis $c = 1.90$ mm. The sample is not a perfect ellipsoid and a demagnetizing factor of $N_{sample} = 0.3755$ was found by optimizing the discontinuous transition of the magnetization in Fig. 5(b), such that the transition occurred over the smallest H_{eq} range. A high-quality sample of a type-I superconducting material should exhibit a crisp transition at H_{cI}. The high-quality nature of our sample [30], along with our μSR measurements showing type-I behavior, justify this optimization procedure for the demagnetization factor. Figure 5(b) shows the magnetization decreases linearly with a slope corresponding to $\chi = -1$ while in the Meissner state. Upon entering the intermediate state the magnetization as a function of H_{eq} is nearly vertical as is expected in a type-I superconductor [31,32]. The change in H_{eq} as the magnitude of the magnetization decreases is due to the thermodynamic critical field being modified from H_c at low field to H_{cI} at fields just below H_{cI}.
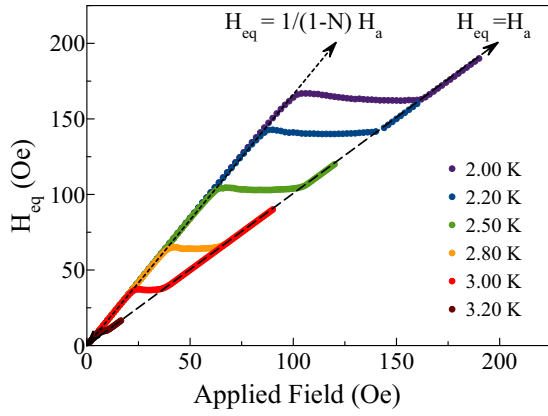
FIG. 6. Internal field at the equator as a function of applied field. In the Meissner state, $H_{eq} = \frac{1}{1-N}H_a$ and the transition to the intermediate state can be identified for applied fields where H_{eq} becomes approximately constant with $H_{cI} \leqslant H_{eq} \leqslant H_c$. In the normal state, $H_{eq} = H_a$.

Figure 6 shows the field at the equator, H_{eq}, of the sample as a function of applied field. This plot matches the expected behavior of H_{eq} for a superconducting ellipsoid given by Refs. [31,32], where there is a linear increase in H_{eq}, while in the Meissner state with $H_{eq} = \frac{H_a}{1-N}$ as H_a is increased to $(1-N)H_{cI}$. In the intermediate state, H_{eq} stays relatively constant with some modification due to the thermodynamic critical field changing from H_c at low fields to H_{cI} near H_{cI}. Above H_{cI}, H_{eq} increases linearly with $H_{eq} = H_a$.

The magnetic susceptibility in applied fields from 10–110 Oe was also measured as a function of temperature using the demagnetization factor found from our previous measurements and is shown in Fig. 7(a). The zero-field cooled (ZFC) measurements (closed circles) show a full magnetic flux expulsion with χ approaching (just below) -1 as T approaches zero, while the FC data (open circles) indicate there is some field being maintained in the sample. Small overlap regions in the intermediate state can be seen where the ZFC and FC results agree. H_{eq} as a function of temperature is shown in Fig. 7(b) again showing small regions of agreement between ZFC and FC. In these small regions of reversibility, H_{cI} can be mapped out as a function of temperature as shown in Fig. 7(c), which can be fit to the Ginzburg-Landau relation,

$$H_c(T) = H_c(0)\left(1 - \left(\frac{T}{T_c}\right)^2\right),\qquad(6)$$

[31,32], yielding $H_c(0) = 252 \pm 2$ Oe and $T_c = 3.249 \pm 0.004$ K.

Combining the results of our μSR measurements (triangles), magnetization versus applied field (black circles) and magnetic susceptibility versus temperature (blue open circles) yields the phase diagram shown in Fig. 8. Overlap regions between μSR and magnetization measurements show good agreement. A fit to Eq. (6) shows good agreement with the experimental data above approximately 0.5 K, with $H_c = 258.5 \pm 0.5$ Oe and $T_c = 3.234 \pm 0.003$ K. The low temperature μSR data shows a slightly flatter than quadratic behavior at low temperature.
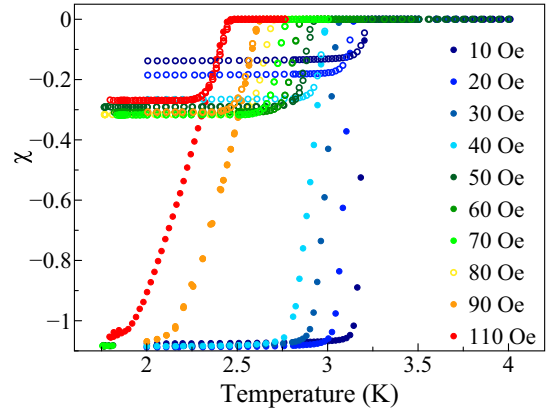
(a)
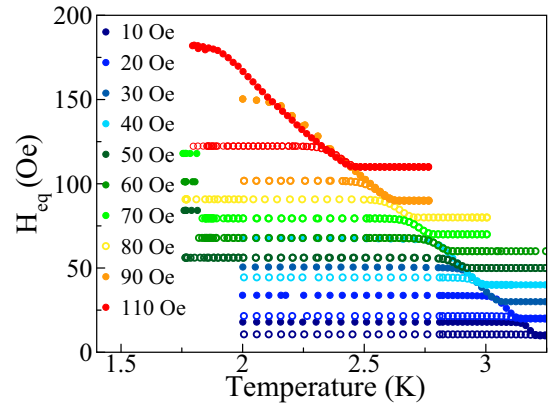
(b)
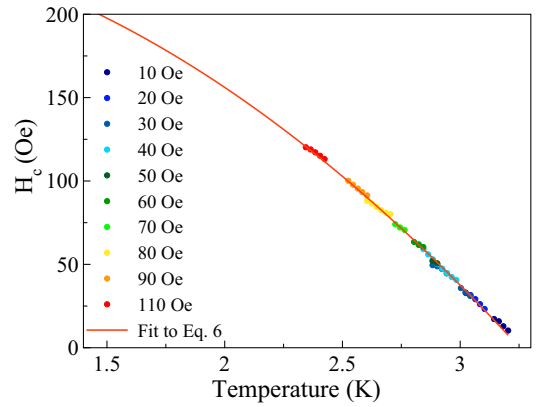
(c)

FIG. 7. (a) Magnetic susceptibility as a function of temperature for applied fields from 10–110 Oe. Zero field cooled (ZFC) (closed circles) and field cooled (FC) (open circle) data show small overlap regions. (b) Equatorial field as a function of temperature for applied fields from 10–110 Oe. ZFC (closed circles) and FC (open circles) show there are small overlap regions. (c) $H_c(T)$ may be mapped out by using data points where the ZFC and FC regions overlap and is fit to Eq. (6), yielding $H_c = 252 \pm 2$ Oe and $T_c = 3.249 \pm 0.004$ K.

The effect of pressure on the system was explored using a pressure cell inserted into the MPMS. Figure 9 shows the results of our magnetization measurements for ambient pressure ($\approx$10 kPa, blue circles) and 450 MPa (red circles) as well as fits to the ambient pressure (blue line) and 450 MPa (red
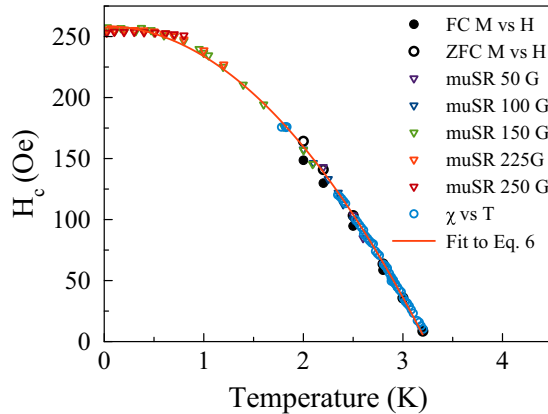
FIG. 8. The field versus temperature phase diagram combining together our μSR (open triangles), magnetization (black circles) and magnetic susceptibility (blue open circles) measurements. A fit to Eq. (6) over the full temperature range and all data sets gives $H_c = 258.6 \pm 0.5$ Oe and $T_c = 3.234 \pm 0.003$ K.

FIG. 9. The magnetic field versus temperature phase diagram from our magnetometry data at 10 kPa (blue circles) and 450 MPa (red circles). A fit to Eq. (6) to the data yields $H_c = 252 \pm 2$ Oe (257 ± 3 Oe) and $T_c = 3.234 \pm 0.004$ K (3.20 ± 0.01 K) for the 10 kPa (450 MPa) data.

line) data. Using Eq. (6), the magnetization measurements at 450 MPa give $H_c = 257 \pm 3$ Oe and $T_c = 3.20 \pm 0.01$ K, while the 10 kPa data gives $H_c = 252 \pm 2$ Oe and $T_c = 3.234 \pm 0.004$ K; a change in T_c of 34 ± 11 mK. Magnetization measurements cannot be performed in low enough temperature to determine if the difference in $H_c(0)$ of 5 ± 4 Oe from a fit to Eq. (6) between the 450 MPa data and ambient pressure data is real. The change in T_c is comparable to the change observed in the elemental type-I superconductors tin (IV), indium, and tantalum which have a decrease in T_c of about 20 mK under the same conditions [48]. This suggests that BeAu is far from a quantum critical point accessible by application of pressure.

IV. CONCLUSION

μSR and demagnetization corrected magnetization measurements were carried out on discs and an ellipsoid of polycrystalline BeAu. Our results show that BeAu is a type-I superconductor with $H_c \approx 258$ Oe and $T_c \approx 3.25$ K. The μSR and magnetization results show consistent values of $H_c(T)$ in the regions where they overlap. A Ginzburg-Landau fit [Eq. (6)] over the entire temperature range and all data sets

give $H_c = 258.6 \pm 0.5$ Oe and $T_c = 3.234 \pm 0.003$ K. Magnetization measurements on an ellipsoid were taken in a pressure chamber at 450 MPa. Fitting only the magnetization data to Eq. (6) yields $H_c = 257 \pm 3$ Oe and $T_c = 3.20 \pm 0.01$ K for the 450 MPa data and H_c 252 ± 2 Oe and T_c 3.234 ± 0.004 K for the 10 kPa pressure data. The reduction in T_c under 450 MPa of pressure in BeAu is comparable to the decrease in T_c observed in the elemental type-I superconductors tin (IV), indium, and tantalum under the same conditions [48]. This suggests that BeAu is far from a quantum critical point accessible by the application of pressure.

Note added. Recently, we became aware of Ref. [59], which reports similar results on BeAu.

[1] E. Bauer and M. Sigrist, *Noncentrosymmetric Superconductors: Introduction and Overview* (Springer, Berlin, 2012).

[2] N. Hayashi, K. Wakabayashi, P. A. Frigeri, and M. Sigrist, Phys. Rev. B **73**, 024504 (2006).

[3] M. Sigrist, D. F. Agterberg, P. A. Frigeri, N. Hayashi, R. P. Kaur, A. Koga, I. Milat, K. Wakabayashi, and Y. Yanase, J. Magn. Magn. Mater. **310**, 536 (2007).

[4] T. Takimoto and P. Thalmeier, J. Phys. Soc. Jpn. **78**, 103703 (2009).

[5] I. Bonalde, W. Brämer-Escamilla, and E. Bauer, Phys. Rev. Lett. **94**, 207002 (2005).

[6] H. Mukuda, T. Fujii, T. Ohara, A. Harada, M. Yashima, Y. Kitaoka, Y. Okuda, R. Settai, and Y. Onuki, Phys. Rev. Lett. **100**, 107003 (2008).

[7] I. Bonalde, R. L. Ribeiro, W. Brämer-Escamilla, G. Mu, and H. H. Wen, Phys. Rev. B **79**, 052506 (2009).

[8] E. Bauer, G. Rogl, X.-Q. Chen, R. T. Khan, H. Michor, G. Hilscher, E. Royanian, K. Kumagai, D. Z. Li, Y. Y. Li, R. Podloucky, and P. Rogl, Phys. Rev. B **82**, 064511 (2010).

[9] M. Nishiyama, Y. Inada, and G.-q. Zheng, Phys. Rev. Lett. **98**, 047002 (2007).

[10] H. Q. Yuan, D. F. Agterberg, N. Hayashi, P. Badica, D. Vandervelde, K. Togano, M. Sigrist, and M. B. Salamon, Phys. Rev. Lett. **97**, 017006 (2006).

[11] M. Isobe, M. Arai, and N. Shirakawa, Phys. Rev. B **93**, 054519 (2016).

[12] V. K. Anand, A. D. Hillier, D. T. Adroja, A. M. Strydom, H. Michor, K. A. McEwen, and B. D. Rainford, Phys. Rev. B **83**, 064522 (2011).

[13] J. A. T. Barker, D. Singh, A. Thamizhavel, A. D. Hillier, M. R. Lees, G. Balakrishnan, D. M. Paul, and R. P. Singh, Phys. Rev. Lett. **115**, 267001 (2015).

[14] A. D. Hillier, J. Quintanilla, and R. Cywinski, Phys. Rev. Lett. **102**, 117007 (2009).

[15] Y. Iwamoto, Y. Iwasaki, K. Ueda, and T. Kohara, Phys. Lett. A **250**, 439 (1998).

[16] K. Sugawara, T. Sato, S. Souma, T. Takahashi, and A. Ochiai, Phys. Rev. B **76**, 132512 (2007).

[17] K. V. Samokhin and V. P. Mineev, Phys. Rev. B **77**, 104520 (2008).

[18] M. A. Khan, A. B. Karki, T. Samanta, D. Browne, S. Stadler, I. Vekhter, A. Pandey, P. W. Adams, D. P. Young, S. Teknowijoyo, K. Cho, R. Prozorov, and D. E. Graf, Phys. Rev. B **94**, 144515 (2016).

[19] D. Singh, A. D. Hillier, A. Thamizhavel, and R. P. Singh, Phys. Rev. B **94**, 054515 (2016).

[20] D. Singh, S. K. P., J. A. T. Barker, D. M. Paul, A. D. Hillier, and R. P. Singh, Phys. Rev. B **97**, 100505 (2018).

[21] P. K. Biswas, H. Luetkens, T. Neupert, T. Stürzer, C. Baines, G. Pascua, A. P. Schnyder, M. H. Fischer, J. Goryo, M. R. Lees, H. Maeter, F. Brückner, H.-H. Klauss, M. Nicklas, P. J. Baker, A. D. Hillier, M. Sigrist, A. Amato, and D. Johrendt, Phys. Rev. B **87**, 180503 (2013).

[22] G. M. Luke, Y. Fudamoto, K. M. Kojima, M. I. Larkin, J. Merrin, B. Nachumi, Y. J. Uemura, Y. Maeno, Z. Q. Mao, Y. Mori, H. Nakamura, and M. Sigrist, Nature **394**, 558 (1998).

[23] J. Xia, Y. Maeno, P. T. Beyersdorf, M. M. Fejer, and A. Kapitulnik, Phys. Rev. Lett. **97**, 167002 (2006).

[24] G. M. Luke, A. Keren, L. P. Le, W. D. Wu, Y. J. Uemura, D. A. Bonn, L. Taillefer, and J. D. Garrett, Phys. Rev. Lett. **71**, 1466 (1993).

[25] P. de Réotier, A. Huxley, A. Yaouanc, J. Flouquet, P. Bonville, P. Imbert, P. Pari, P. Gubbens, and A. Mulders, Phys. Lett. A **205**, 239 (1995).

[26] Y. Aoki, A. Tsuchiya, T. Kanayama, S. R. Saha, H. Sugawara, H. Sato, W. Higemoto, A. Koda, K. Ohishi, K. Nishiyama, and R. Kadono, Phys. Rev. Lett. **91**, 067003 (2003).

[27] Y. Aoki, T. Tayama, T. Sakakibara, K. Kuwahara, K. Iwasa, M. Kohgi, W. Higemoto, D. E. MacLaughlin, H. Sugawara, and H. Sato, J. Phys. Soc. Jpn. **76**, 051006 (2007).

[28] V. G. Yarzhemsky and V. I. Nefedov, Phys. Solid State **51**, 448 (2009).

[29] A. Bhattacharyya, D. Adroja, N. Kase, A. Hillier, J. Akimitsu, and A. Strydom, Sci. Rep. **5**, 12926 (2015).

[30] A. Amon, E. Svanidze, R. Cardoso-Gil, M. N. Wilson, H. Rosner, M. Bobnar, W. Schnelle, J. W. Lynn, R. Gumeniuk, C. Hennig, G. M. Luke, H. Borrmann, A. Leithe-Jasper, and Y. Grin, Phys. Rev. B **97**, 014501 (2018).

[31] P.-G. de Gennes, *Superconductivity of Metals and Alloys*, Advanced Book Classics (Advanced Book Program, Perseus Books, Reading, MA, 1999).

[32] M. Tinkham, *Introduction to Superconductivity*, 2nd ed. (McGraw-Hill, New York, 1975).

[33] *Collected Papers of L. D. Landau*, edited by D. T. Haar (Pergamon Press INC, New York, 1965), pp. 365–379.

[34] V. S. Egorov, G. Solt, C. Baines, D. Herlach, and U. Zimmermann, Phys. Rev. B **64**, 024524 (2001).

[35] E. Svanidze and E. Morosan, Phys. Rev. B **85**, 174514 (2012).

[36] A. Yamada, R. Higashinaka, T. D. Matsuda, and Y. Aoki, J. Phys. Soc. Jpn. **87**, 033707 (2018).

[37] J. Bekaert, S. Vercauteren, A. Aperis, L. Komendová, R. Prozorov, B. Partoens, and M. V. Milošević, Phys. Rev. B **94**, 144506 (2016).

[38] M. V. Salis, P. Rodière, H. Leng, Y. K. Huang, and A. de Visser, J. Phys.: Condens. Matter **30**, 505602 (2018).

[39] U. Gottlieb, J. C. Lasjaunias, J. L. Tholence, O. Laborde, O. Thomas, and R. Madar, Phys. Rev. B **45**, 4803 (1992).

[40] M. Kriener, T. Muranaka, J. Kato, Z.-A. Ren, J. Akimitsu, and Y. Maeno, Sci. Technol. Adv. Mater. **9**, 044205 (2008).

[41] M. Smidman, A. D. Hillier, D. T. Adroja, M. R. Lees, V. K. Anand, R. P. Singh, R. I. Smith, D. M. Paul, and G. Balakrishnan, Phys. Rev. B **89**, 094509 (2014).

[42] K. Wakui, S. Akutagawa, N. Kase, K. Kawashima, T. Muranaka, Y. Iwahori, J. Abe, and J. Akimitsu, J. Phys. Soc. Jpn. **78**, 034710 (2009).

[43] F. Honda, I. Bonalde, K. Shimizu, S. Yoshiuchi, Y. Hirose, T. Nakamura, R. Settai, and Y. Ōnuki, Phys. Rev. B **81**, 140507 (2010).

[44] R. Settai, I. Sugitani, Y. Okuda, A. Thamizhavel, M. Nakashima, Y. Ōnuki, and H. Harima, J. Magn. Magn. Mater. **310**, 844 (2007).

[45] N. Kimura, K. Ito, K. Saitoh, Y. Umeda, H. Aoki, and T. Terashima, Phys. Rev. Lett. **95**, 247004 (2005).

[46] T. Yasuda, H. Shishido, T. Ueda, S. Hashimoto, R. Settai, T. Takeuchi, T. D Matsuda, Y. Haga, and Y. Nuki, J. Phys. Soc. Jpn. **73**, 1657 (2004).

[47] Y. Mizuguchi, F. Tomioka, S. Tsuda, T. Yamaguchi, and Y. Takano, Appl. Phys. Lett. **93**, 152505 (2008).

[48] L. D. Jennings and C. A. Swenson, Phys. Rev. **112**, 31 (1958).

[49] A. Suter and B. M. Wojek, Physics Procedia **30**, 69 (2012).

[50] L. D. Landau and E. M. Lifshitz, *Electrodynamics of Continuous Media* (Pergamon Press INC, New York, 1983), p. 460.

[51] E. Andrew, Proc. R. Soc. London A **194**, 98 (1948).

[52] A. Fortini and E. Paumier, Phys. Rev. B **5**, 1850 (1972).

[53] J. D. Livingston, Phys. Rev. **129**, 1943 (1963).

[54] J. D. Livingston, J. Appl. Phys. **34**, 3028 (1963).

[55] R. P. Huebener, *Magnetic Flux Structures in Superconductors* (Springer-Verlag, Berlin, 1979).

[56] J. E. Sonier, J. H. Brewer, and R. F. Kiefl, Rev. Mod. Phys. **72**, 769 (2000).

[57] J. A. Osborn, Phys. Rev. **67**, 351 (1945).

[58] M. Beleggia, M. D. Graef, and Y. Millev, Philos. Mag. **86**, 2451 (2006).

[59] D. Singh, A. D. Hillier, and R. P. Singh, Phys. Rev. B **99**, 134509 (2019).